PANAMGEO CHILE 2024
17th PAN-AMERICAN CONFERENCE ON SOIL MECHANICS AND GEOTECHNICAL ENGINEERING | 2nd LATIN-AMERICAN REGIONAL CONFERENCE OF IAEG
LA SERENA • CHILE / NOVEMBER 12 - 16, 2024

Proceedings of the 17th Pan-American Conference on Soil Mechanics and Geotechnical Engineering (XVII PCSMGE), and 2nd Latin-American Regional Conference of the International Association for Engineering Geology and the Environment (IAEG), La Serena Chile, 2024.

Evaluation of the radiation damping in tailings dams

Evaluación del amortiguamiento por radiación en muros de relaves

Javier Ubilla
Nava Consulting, Chile, javier.ubilla@nava.cl

Esteban Sáez
Department of Structural and Geotechnical Engineering, Pontificia Universidad Católica de Chile, Chile.

ABSTRACT: The dynamic deformation analysis has become a standard practice to evaluate the tailings dams physical stability during earthquakes. Several publications describe these types of numerical models, including the nonlinear soil behavior producing hysteretic damping. However, little discussion is available regarding the radiation damping acting in tailings dams, which is usually unquantified in numerical modelling. The radiation damping through the dam/foundation and dam/impoundment interfaces is analyzed in this article using the software FLAC, for various dam upstream slopes, and varying the geotechnical properties of the foundation material and the tailings in the impoundment. The results show that the radiation damping is a significant component of the dam dynamic response, with damping ratios that can reach values as high as 20% for certain dam configurations.

KEYWORDS: Radiation damping, tailings dam, dynamic analysis, seismic analysis.

1 INTRODUCTION

The implementation of computational models representing Tailings Storage Facilities, TSF, for the evaluation of their physical stability has become a standard practice in countries with significant mining activity. For TSFs that exceed a certain threshold in terms of height, storage capacity, or consequence of failure, regulations of different earthquake-prone countries mandate or recommend a dynamic deformation analysis to evaluate the seismic behavior of the tailings dam (ANCOLD, 2019; CDA, 2013; ICMM, 2021; SERNAGEOMIN, 2007).

Several publications are available presenting the results of dynamic deformation analyses (e.g. Psarropoulos et al., 2008; Chakraborty et al., 2011; Ferdosi et al., 2015; Borja et al., 2016; Naeini et al., 2018; Vargas, 2019; Shuttle at al., 2021). For this kind of analyses, geotechnical engineering practitioners must represent the properties and behavior of the materials that compose the dam, such as mine waste rockfill, tailings sand, or quarry material, usually involving sophisticated constitutive models to represent the nonlinear behavior of the dam fill materials. This effort includes the calibration of the model´s parameters, commonly achieved by numerically reproducing the results of a stress-strain laboratory test, e.g. monotonic or cyclic triaxial compression or direct simple shear tests, and adjusting the model parameters until achieving a reasonable similarity between the laboratory results, and the numerical simulation. Usually, during TSF construction, strict protocols are stablished for the selection and compaction effort of the dam fill materials, therefore, a reasonable material uniformity and geotechnical characterization can be achieved and implemented in the numerical model.

However, this is usually not the case for the foundation material and the tailings in the impoundment. The foundation material may have a wide range of properties in horizontal extension and depth, depending on the site conditions. Also, a significant material variability can be expected for the tailings in the impoundment (Villavicencio et al., 2011). Given a certain range of properties, the specialist must select a representative set of geotechnical parameters as input in the numerical model, which is not an easy task. In fact, Paull et al. (2020) carried out a set of dynamic deformation analyses of embankments sitting on non-uniform alluvial and liquefiable material and compared the results with additional models in which uniform alluvium properties were considered. They concluded that the representative uniform geotechnical properties are generally between the 30th and 60th percentile of the properties range, depending on the aspect of the dam behavior of interest.

In a numerical model, the dynamic behavior of a tailings dam is the result of the dam´s characteristics, as well as the nature of the interaction of the dam with the foundation materials and the tailings in the impoundment. One aspect of this dynamic interaction is in the form of radiation damping, which is dependent on the impedance ratio between adjacent materials, as well as the model geometry, described below.

2 RADIATION DAMPING

During seismic events, the seismic waves travel through the bedrock, and then through the soil strata, before reaching the soil surface. At each of these boundaries, i.e. bedrock-soil and between soil layers, a portion of the incident wave is transmitted to the following layer in the direction of propagation, and a portion is reflected back, as presented in Figure 1 for a one-dimensional analysis.

The waves that travel downward, and reach the bedrock, will dissipate in this infinite half-space, and never come back to the soil strata. This “leakage” of energy generates radiation damping, which is in addition of the hysteretic damping that the materials produce depending on its nonlinear cyclic stress-strain behavior. Both sources of damping contribute to reduce the soil dynamic response.

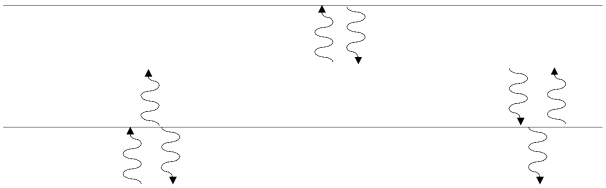

Figure 1. Waves interaction with a geotechnical boundary.

For an incident wave reaching perpendicularly a boundary between two different layers, a to b, the proportion of the wave that is transmitted and reflected depends on the impedance, ρV, of each layer, and more specifically on the impedance ratio, α, between layers, as presented in Equation 1.

$$\alpha = \frac{(\rho V)_b}{(\rho V)_a} \quad (1)$$

Where ρ is the mass density of the stratum and V is the wave velocity, V_s or V_p, for shear waves or pressure waves, respectively. The impedance ratio is a fundamental aspect in the analysis of wave propagation through soil interfaces. In fact, Kramer (1996) shows that the amplitude of the reflected wave, $A_{reflected}$, normalized by the amplitude of the incident wave, $A_{incident}$, is a function of the impedance ratio (Equation 2):

$$\frac{A_{reflected}}{A_{incident}} = \frac{1-\alpha}{1+\alpha} \quad (2)$$

The absolute value of the wave amplitude ratio in Equation 2 is plotted in Figure 2. For α < 1, i.e. wave propagating from a stiff to a soft layer, the amplitude of the reflected wave increases with decreasing α, with a limiting value of α = 0, meaning that there is no media beyond the boundary (soil surface), and the incident wave is fully reflected. The same occurs for α > 1, i.e. wave propagating from a soft to a stiff layer, the amplitude of the reflected wave increases with increasing α, with a limiting value of α = ∞, representing a perfectly rigid boundary, and the incident wave is fully reflected. When α = 1 there is no impedance contrast between the two layers, and the amplitude of the reflected wave is zero, meaning that the wave is fully transmitted.

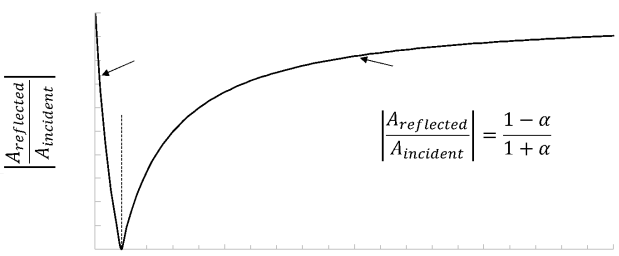

Figure 2. Reflected wave ratio for different values of α.

The same concept can be applied to a tailings dam. Assuming that the foundation material is stiffer, and that the tailings in the impoundment are softer than the dam material, the α < 1 condition can be representative of the boundary between the dam upstream slope and the tailings in the impoundment, while the α > 1 condition can be representative of the boundary between the dam base and the foundation material. The waves traveling through these boundaries could be of compressional or shear nature, depending on the dam movement in this dynamic interaction with its foundation soil and contained tailings.

The radiation damping also occurs in tailings storage facilities, through the boundaries between the dam, the tailings in the impoundment, and the foundation. During the dam vibration, the radiation damping dissipates energy from the dam to the tailings and foundation materials through a combination of compression - extension and shear waves, similarly to the case of machine foundations, but with the main difference of the flexibility of the dam versus a rigid machine foundation assumed in the analytical solutions. The question is how important the radiation damping is for the overall dam dynamic response, and what are the key factors to consider.

A series of numerical models were developed to quantify the radiation damping, as a contributing factor in the stability of a tailings dam. A simple configuration is analyzed, consisting of three materials: foundation, dam, and tailings, as shown in Figure 3. During an earthquake, there is input movement transmitted from the foundation to the dam and tailings. After that, there is a dynamic interaction between the foundation, the dam, and the tailings, in which waves are reflected and transmitted at the boundaries between these tree materials. This is schematically represented in Figure 3.

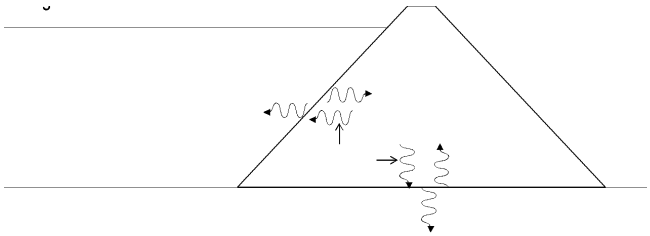

Figure 3. Radiation damping in a tailings dam during free dam vibration.

In this paper, the radiation damping is analyzed from the dam perspective, and the energy transmitted from the dam to the foundation, and from the dam to the tailings, during free dam vibration (Figure 3), is evaluated. Different geometry configurations and material properties are included in the study, as described next.

3 CONCEPTUAL MODELS OF TAILINGS DAMS

3.1 *Model description.*

With the objective to evaluate the radiation damping in tailings dams, four numerical models were developed using the commercially available software FLAC v.8 (Fast Lagrangian Analysis of Continua). The numerical models consist in a foundation with 1300 m width and 100 m height, a tailings dam with 100 m height, 20 m crest width, 2H:1V downstream slope, and variable upstream slope: 2H:1V, 1H:1V, 0.5H:1V and 0H:1V, or vertical upstream slope. In all the cases, the tailings

impoundment had 95 m height, or 5 m freeboard with respect to the dam crest, as presented in Figure 4. In the numerical model, the continuum is discretized in square zones, with a size of 1 m.

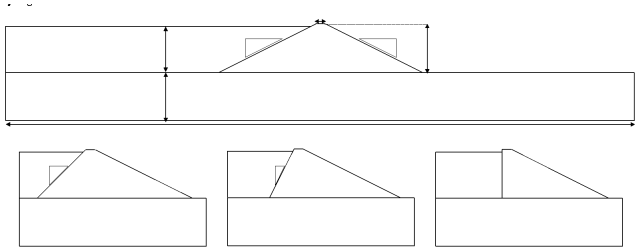

Figure 4. Dam geometries considered in the study: a) 2H:1V upstream slope, b) 1H:1V upstream slope, c) 0.5H:1V upstream slope, d) Vertical upstream slope.

The boundary conditions of the model were selected to represent the infinite half space in the lateral and downward directions. The free-field condition was imposed at the lateral boundaries of the model, while the quiet boundary was imposed at the base of the model. These types of boundaries are described in the FLAC manual (Itasca, 2019).

The purpose of the quiet boundary is to simulate an infinite half-space, by absorbing the downward propagating waves. The quiet boundary scheme involves dashpots attached independently to the base of the model in the normal and shear directions. The dashpots provide viscous normal and shear tractions dependent on the mass density and the boundary wave velocity.

The free-field lateral boundary consists of a one-dimensional "column" of unit width, simulating the behavior of the extended medium. If the main-grid motion differs from that of the free field, for example due to the dam vibration, then this boundary condition includes dashpots to absorb energy in a similar manner to the action of quiet boundaries.

3.2 *Material properties.*

The linear elastic constitutive model was selected for all materials, without any Rayleigh or hysteretic type of damping. The use of a linear elastic model has the purpose to allow the exclusive evaluation of the radiation damping, as the only possible source of energy dissipation for the model, and particularly for the tailings dam. Table 1 presents the properties of the dam, foundation, and tailings. The properties have been selected arbitrarily, within a realistic range. The shear modulus, G, for the dam and the tailings increases with the vertical effective confining pressure, as per Equation 3.

$$G = G_0 P_a \sqrt{\frac{\sigma_v`}{P_a}} \quad (3)$$

Where $\sigma_v`$ is the effective vertical stress, Pa is the atmospheric pressure (1 atm = 101.33 kPa), and G_0 is a dimensionless constant. Table 1 also includes the shear wave velocity at a confining pressure equivalent to 1 Pa, calculated as per Equation 4, as a function of the corresponding shear modulus and the mass density, ρ.

$$V_{s1} = \sqrt{\frac{G(\sigma_v`=1\ atm)}{\rho}} \quad (4)$$

The shear modulus of the dam was selected such that its value at a vertical effective stress of 1 atm is V_{s1} = 300 m/s, representing a compacted granular fill, with a limited degradation due to cyclic loading. The shear modulus for the tailings was selected such that V_{s1} = 10 m/s, which may correspond to the residual properties of a material at or close to a liquefied state. In the opinion of the authors, this is within the range of values commonly assumed in dynamic deformation analyses. It is noted that there is a significant impedance contrast between the dam and the foundation materials, and the dam and tailings materials.

Table 1. Model's geotechnical properties

	Dam	Foundation	Tailings
Constitutive Model	Elastic	Elastic	Elastic
Humidity	Dry	Dry	Saturated
Mass Dry Density, ρ (kg/m³)	1,835	2,500	1,835
Shear Modulus, G (kN/m²)	Equation 3	10,000,000	Equation 3
Shear Modulus Parameter, G_0	1,630	-	1.8
Poisson`s Ratio, μ	0.3	0.2	0.49
Shear Wave Velocity, V_{s1} (m/s)	300	2,000	10
Compressional Wave Velocity, V_{p1} (m/s)	561	3,266	71

The water in the tailings impoundment is modeled as a pore water pressure, reducing the effective stress in the tailings, while the compressional wave velocity, V_p, is evaluated from the shear wave velocity and the Poisson`s ratio, $(V_p/V_s)^2=(2-2\mu)/(1-2\mu)$, as presented in Table 1.

A Ricker wavelet has the property to include a wide range of frequencies in a relatively short signal. This type of wavelet was used to excite each model and evaluate the transfer function, as the ratio between the Fourier spectrum of the horizontal acceleration at the crest and the base of the dam. This allowed to obtain the fundamental period of vibration of each dam configuration, T_1, as presented in Figure 5, which increases with the dam upstream slope.

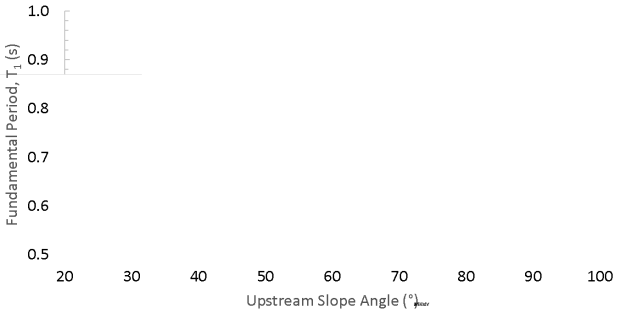

Figure 5. Fundamental period for different dam upstream slope angle.

4 RADIATION DAMPING EVALUATION

4.1 *Methodology.*

To evaluate the radiation damping of each dam geometry presented in Figure 4, the models were subjected to a horizontal motion applied at the base of the Foundation material. The input motion consisted of a sinusoidal wave with the same period as the T_1 value of each corresponding dam configuration (Figure 5). In this way, the models are excited only at their first natural period of vibration and can be treated as a single degree of freedom system.

The damping ratio, ξ, of the dam was obtained by analyzing the amplitude decay of the free vibration sinusoidal dam crest

movement, after the end of the input motion, using the following expression:

$$A(t) = A_0 e^{-\omega_1 \xi t} \quad (5)$$

Where A(t) is the amplitude of the movement, A_0 is the initial amplitude (at t = 0), ω_1 is the first natural frequency, $\omega_1 = 2\pi/T_1$, and ξ represents the damping ratio, defined as the damping of the system divided by the critical damping. As previously mentioned, a linear elastic constitutive model was selected for the dam, foundation, and tailings materials. This modeling consideration was adopted to isolate the radiation damping, as the only possible source of damping, allowing its quantification.

Figure 6 presents and example of the horizontal acceleration response at the middle of the crest of the dam. The term $-\omega_1\xi$ can be evaluated by curve fitting the logarithmic decay of the dynamic free vibration of the dam, after the sinusoidal input has ended. Also, given the period of the free vibration, the frequency can be evaluated as $\omega_1 = 2\pi/T_1$ then, the total damping ratio, ξ_{total}, can be obtained, corresponding to radiation damping only.

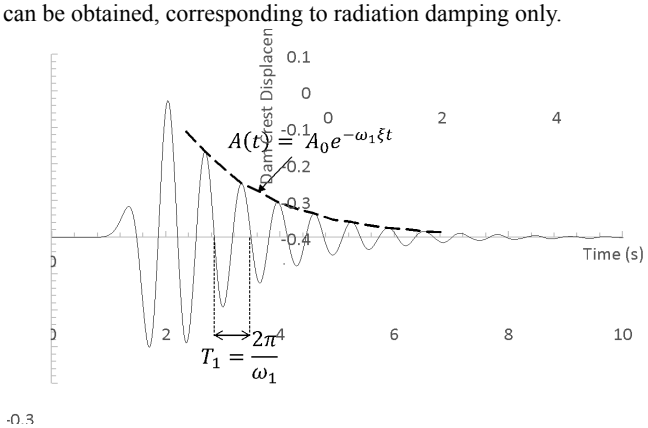

Figure 6. Example of logarithmic decay of dam crest acceleration.

Figure 7 presents the total radiation damping, ξ_{total}, for each dam configuration. This total radiation damping has the contribution from the radiation damping through the foundation, and through the tailings in the impoundment. The results show an increasing tendency with the dam`s upstream slope angle, reaching ξ_{total} = 12.85% for the vertical upstream slope condition.

The movement of the boundary between the dam and the foundation, or the dam and the tailings, has a component parallel to the boundary, mainly associated with shear "s" waves, and perpendicular to the boundary, mainly associated with compressional "p" waves. Therefore, four components of ξ_{total} can be identified, as presented in Figure 8.

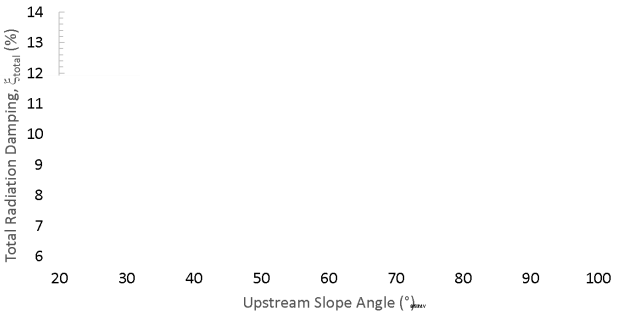

Figure 7. Total radiation damping for different upstream slope angles.

Considering that only the T_1 period is excited, and that the single degree of freedom equations are valid, the total radiation damping can be idealized as the sum of the foundation and tailings damping contributions, as indicated in Equation 6 through Equation 8:

$$\xi_{total} = \xi_{foundation} + \xi_{tailings} \quad (6)$$

$$\xi_{foundation} = \xi_{foundation-p} + \xi_{foundation-s} \quad (7)$$

$$\xi_{tailings} = \xi_{tailings-p} + \xi_{tailings-s} \quad (8)$$

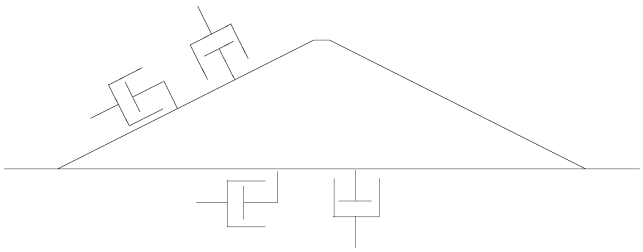

Figure 8. Idealization of the radiation damping dashpots.

The following sections presents an evaluation of each component of the total radiation damping, using numerical models, for each dam configuration in Figure 4.

4.2 *Radiation damping through the foundation.*

To evaluate the radiation damping through the foundation, the radiation damping through the tailings is eliminated, so the incident wave from the dam to the tailings is fully reflected, and none of it is transmitted (Figure 3). This is achieved by replacing the tailings in the impoundment by an equivalent hydrostatic pressure, maintaining the confinement that the tailings produce on the foundation and the dam upstream face.

Figure 9 presents the mayor principal stress, in kPa, in the model with equivalent pressure (Figure 9a) and with the tailings explicitly included in the model (Figure 9b). It can be noted that the stress distribution in the dam and foundation is almost identical in both models, meaning that the equivalent hydrostatic pressure, perpendicular to the upstream dam slope and foundation surface, correctly represents the pressure exerted by the tailings. There may be a shear stress component, produced by the tailings in the impoundment, acting on the dam upstream face of the dam, and not captured by the equivalent hydrostatic pressure approach, however, the numerical models show that this shear component is negligeable.

The equivalent hydrostatic pressure allows that all the pressure-dependent properties of the dam are maintained (Table 1). The same equivalency was done for all the dam geometries considered in this study.

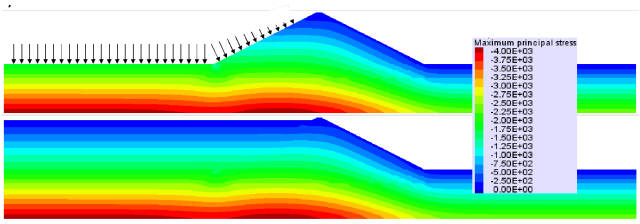

Figure 9. Maximum principal stress distribution: a) tailings modeled as equivalent pressure and b) tailings modeled explicitly.

Replacing the tailings by an equivalent pressure has the consequence that no radiation damping can occur through the tailings in the impoundment, and the only source of radiation damping is through the foundation of the dam. Figure 10 presents the radiation damping under this configuration, $\xi_{foundation}$, as a function of the length of the dam/foundation boundary.

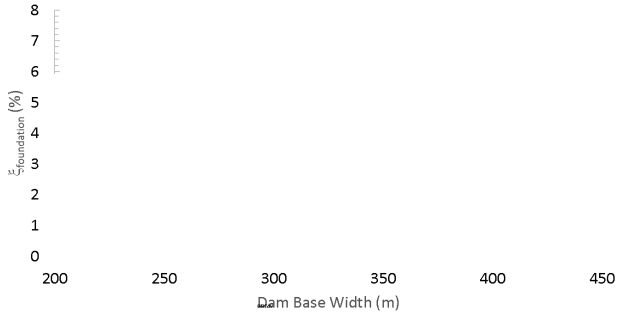

Figure 10. Radiation damping through dam-foundation boundary.

Even though the input motion is horizontal, the dam movement is not purely horizontal, there is a significant vertical component, due to the dam flexibility and multiple wave reflections at the dam edges. Figure 11 presents the horizontal and vertical particle velocity pattern at selected points of the dam/foundation boundary, for the free-vibration cycles after the dynamic input has ended. It is clear the vertical component of the dam movement, that increases from the center to the upstream and downstream sides of the dam section.

At the contact between the dam and the foundation, the horizontal component of the movement dissipated energy in the form of shear waves, and the vertical component of the movement dissipates energy in the form of compressional waves. Both shear and compressional waves components contribute to the total value of $\xi_{foundation}$ presented in Figure 10, however, it is not straightforward to evaluate in what proportion.

With the objective to decouple the vertical and horizontal components of $\xi_{foundation}$, the numerical models were repeated, but including a restriction to the nodes at the contact between the dam and the foundation, so they can only move in the horizontal direction. In this way, mainly the shear component of the radiation damping was allowed, and the compressional component of the radiation damping can be calculated as (Equation 9). This is valid because a linear elastic constitutive model was implemented, and the principle of superposition applies.

$$\xi_{foundation-p} = \xi_{foundation} - \xi_{foundation-s} \quad (9)$$

Based on this analysis, the values $\xi_{foundation-s}$ and $\xi_{foundation-p}$, along with the total damping through the foundation, $\xi_{foundation}$, were calculated and presented in Figure 12 as a function of the dam upstream slope. Depending on the dam geometry, the radiation damping through the foundation vary between 3.1% to 7.2%. It is also observed that $\xi_{foundation-s}$ could be smaller or larger that $\xi_{foundation-p}$, depending on the angle of the upstream slope of the dam.

The damping values in Figure 12 are significant and have an impact reducing the amplitude of the overall dam`s dynamic response. This result also shows the importance of correctly model the foundation stiffness properties, to avoid overestimate or underestimate the value for $\xi_{foundation}$. To illustrate this effect, the 2H:1V model was repeated, but varying the shear and compressional wave velocities, V_s and V_p respectively, of the foundation material and maintaining the Poisson ratio at 0.2.

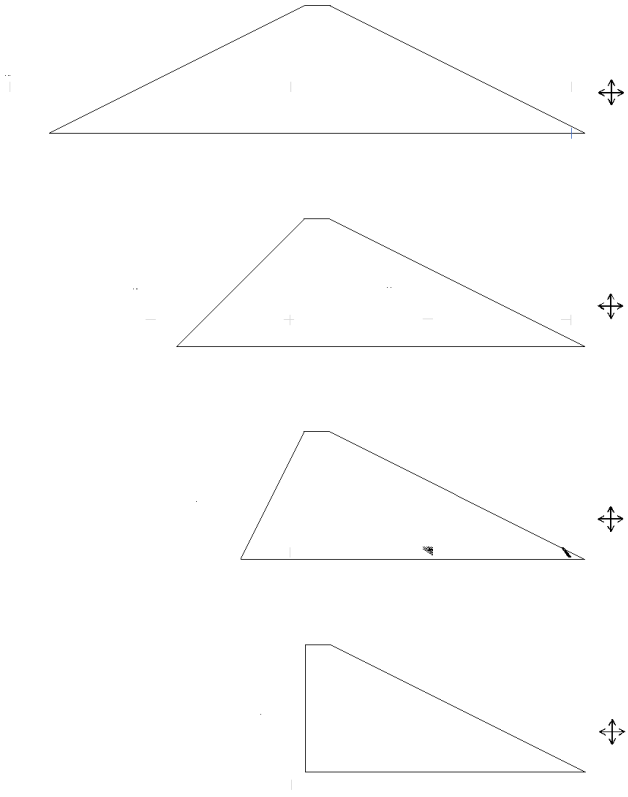

Figure 11. Particle velocity pattern in the dam-foundation boundary during dam free vibration for different dam upstream slopes.

The variation of $\xi_{foundation}$ with the foundation stiffness, expressed in terms of V_s, is presented in Figure 13, for V_s = 1000 m/s, V_s = 2000 m/s, and V_s = 3000 m/s. As expected, the damping through the foundation of the dam decreases as the foundation material increases its stiffness and the impedance ratio also

increases, consistent with the trend of the branch $\alpha > 1$ in Figure 2.

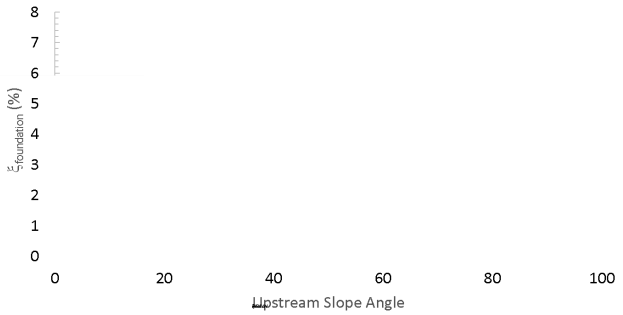

Figure 12. Shear and compressional wave contribution to the radiation damping through the dam-foundation boundary.

The results of Figure 13 show that the range of variation of the radiation damping with the foundation stiffness is very important, meaning that the foundation stiffness used in dynamic deformation models will have an impact in the dam dynamic performance. The results also show that the radiation damping decreases with increasing foundation stiffness, therefore, from an energy radiation perspective, it is conservative to overestimate the foundation stiffness, and not to underestimate it.

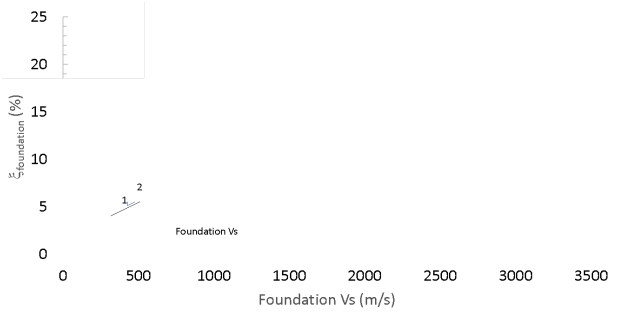

Figure 13. Radiation damping through the dam-foundation boundary for different foundation stiffness.

4.3 *Radiation damping through the tailings in the impoundment.*

The dam vibration induces movement of the tailings in the impoundment. This is evident in Figure 14, which shows displacement vectors of the tailings next to the upstream face of the dam in sequential times T_1 through T_4, during the dam vibration. From this figure, it can be observed that there is energy transferred from the dam to the tailings.

From the total damping, ξ_{total}, presented in Figure 7, the damping through the foundation, $\xi_{foundation}$, previously evaluated (Figure 12), can be subtracted, obtaining the damping through the tailings, $\xi_{tailings}$ (Equation 6). This is further discussed in Section 6 of this article. The results are presented in Figure 15, showing that $\xi_{tailings}$ varying from about 0.8% to 9.7% for different dam upstream slopes.

In Figure 15 it is observed that in $\xi_{tailings}$ there is a tendency to increase with the steeper upstream slope of the dam. To understand the source of this effect, it is useful to observe the horizontal and vertical velocity pattern during the dam free vibration at five selected points on the dam upstream slope, named 1 through 5 from bottom to top, as presented in Figure 16.

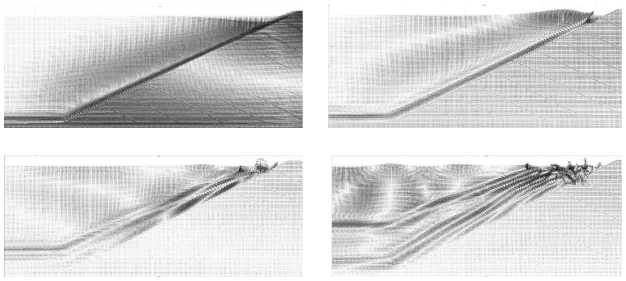

Figure 14. Tailings movement induced by dam vibration for times T1 < T2 < T3 < T4.

There is an angle between the velocity profile and the upstream surface of the dam, therefore, there is a component of the surface velocity that produces compressional waves, $P_{component}$, and a component that produces shear waves, $S_{component}$, as presented in Figure 17. The ratio $P_{component}/S_{component}$ increases with the slope of the upstream face of the dam, meaning that, as the slope increases, the $P_{component}$ becomes predominant.

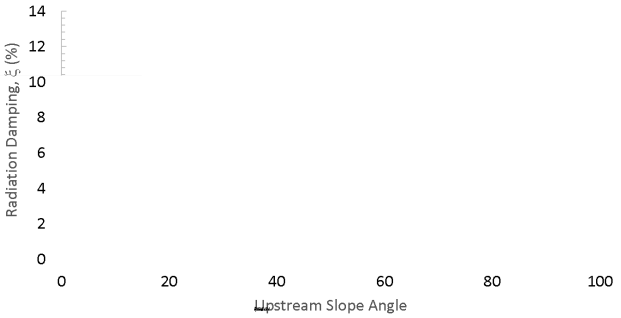

Figure 15. Radiation damping through the foundation and through the tailings.

The amplitude of the upstream surface particle velocity increases from the bottom to the top of the dam, as presented in Figure 16, therefore the contribution to the damping also increases from bottom to top.

For all the dam configurations, five control points have been used to evaluate the upstream slope particle velocity, from Nº1 near the upstream toe to Nº5 near the crest of the dam. For comparison purposes, it is convenient to multiply the $P_{component}/S_{component}$ ratio by the normalized amplitude of the of the velocity pattern, L_i/L_5, where L_i is the particle velocity amplitude of the i point of the upstream slope, as presented in Figure 17.

The ψ parameter is proposed to evaluate the compressional and shear waves contribution to the radiation damping on the upstream slope of the dam:

$$\psi = \frac{P_{component}}{S_{component}} * \frac{L_i}{L_5} \qquad (10)$$

Figure 18 presents the ψ profile for the different upstream slopes considered. The parameter ψ increases with the steepness of the dam upstream slopes, due to an increase of the $P_{component}/S_{component}$ ratio. This means that the waves induced in the tailings gradually shifts from a predominantly shear wave to a predominantly compressional wave as the upstream slope increases.

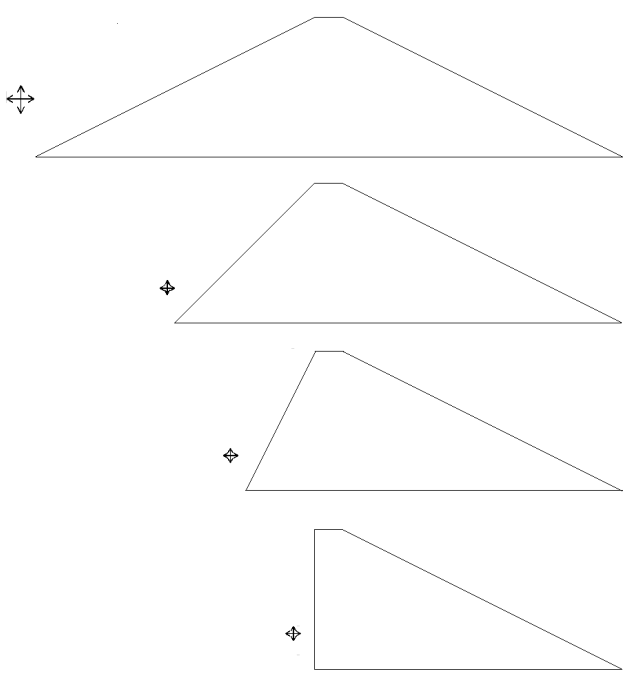

Figure 16. Particle velocity pattern in the dam-tailings boundary during dam free vibration for different dam upstream slopes.

The tailings compressional wave velocity is larger than the shear wave velocity, in fact $V_{p1}/V_{s1} = 7.1$ (Table 1). This produces that, for the dam-tailings dynamic interaction, the impedance ratio for the compressional wave component, α_{DTp} is larger than the shear wave component, α_{DTs}:

$$\alpha_{DTs} = \frac{(\rho V_{s1})_{Tailings}}{(\rho V_{s1})_{Dam}} = 0.03 \text{ and}$$

$$\alpha_{DTp} = \frac{(\rho V_{p1})_{Tailings}}{(\rho V_{p1})_{Dam}} = 0.12$$

As the reflected wave decreases with increasing the impedance ratio for the $\alpha < 1$ branch in Figure 2, there is a larger percentage of the compressional wave, in comparison with the shear wave, that can go through the boundary between the dam and the tailings.

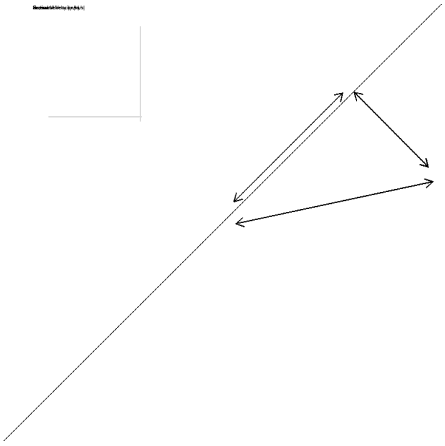

Figure 17. Shear and compressional components of the dam upstream slope velocity.

As the ψ parameter increases with the upstream slope of the dam, this produces the corresponding increase in the $\xi_{tailings}$ presented in Figure 15, reaching almost 10% for a vertical upstream slope, which is a significant contribution to reduce the dam´s dynamic response.

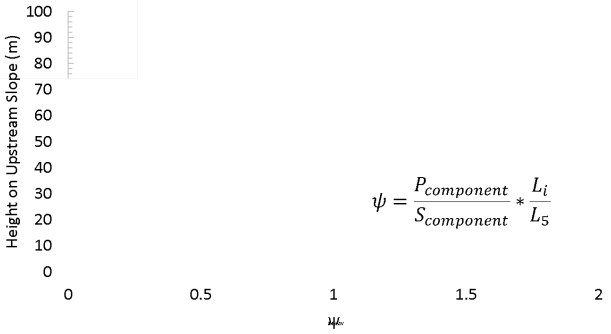

Figure 18. Variation of y parameter for different dam upstream slope angles.

The value of $\xi_{tailings}$ was evaluated for different stiffness of the tailings, represented through the V_{s1} parameter, for the case 2H:1V upstream slope. The V_{s1} values considered are 50 m/s and 100 m/s, in addition to the 10 m/s previously described. In particular, V_{s1} = 100 m/s corresponds to a very loose sandy or silty soil (Youd et al., 2001), which may be representative of the stiffness of the tailings in the impoundment, but with a limited degradation due to cyclic loading.

Figure 19 presents the results, where a significant increase of the damping through the tailings occurs with increasing the tailings stiffness as the impedance contrast drops. The results are consistent with the $\alpha < 1$ branch in Figure 2, where the amplitude of the reflected wave decreases with increasing α, and more energy goes through the dam/tailings boundary. The results in Figure 19 shows the importance of modelling the tailings dynamic behavior and pore water pressure buildup, eventually leading to liquefaction, with the subsequent progressive reduction in the tailings stiffness. This will affect the radiation damping through the dam/tailings interface, with a larger influence on the dam overall dynamic response for dams with steeper upstream slopes.

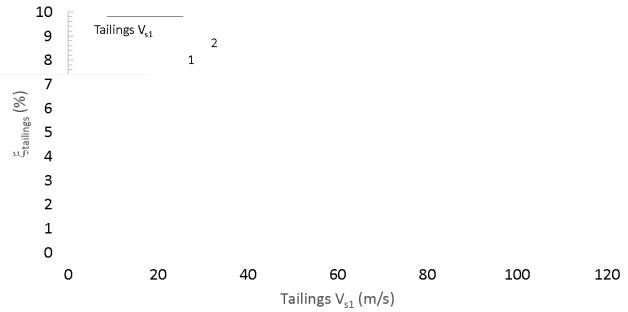

Figure 19. Variation of the radiation damping through the dam-tailings boundary with the tailings stiffness.

The geometry of the dam in Figure 4d represents a centerline raise of the tailings dam. In this case, a more realistic configuration of a centerline raise dam is presented in Figure 20, where the upstream slope geometry corresponds to ten stages of dam raises with a trapezoidal shape. This model was subjected to the sinusoidal wave previously described, obtaining:

$$\xi_{tailings\ center\ line} = 20.9\%$$

This radiation damping through the tailings is about twice the value obtained for the geometry in Figure 4d, $\xi_{tailings} = 9.7\%$. It is presumed that this difference is due to the increase of the length of the boundary between the dam and the tailings, and likely a more significant $P_{component}/S_{component}$ ratio.

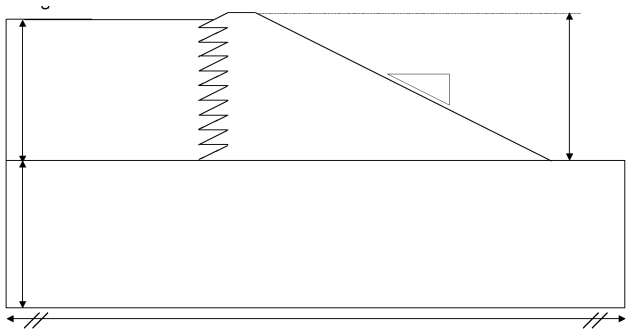

Figure 20. Geometry of a centerline raise tailings dam.

5 DAM SDOF IDEALIZATION

In the previous sections, the $\xi_{foundation}$ was evaluated for a dam configuration without the tailings, which were replaced by an equivalent hydrostatic pressure, therefore $\xi_{tailings} = 0$. Then, the tailings were explicitly included in the model, allowing the evaluation of the total radiation damping, ξ_{total}, and the damping contribution from the tailings was evaluated as $\xi_{tailings} = \xi_{total} - \xi_{foundation}$. The hypothesis behind this equation is that the presence of the tailings, or the equivalent pressure, only affects the damping, *c*, acting on the dam idealized as a SDOF system, without significantly affecting the respective mass, *m*, and spring constant, *k*.

To evaluate this hypothesis the well-known SDOF equations were used to reproduce the horizontal acceleration of the dam crest during free vibration. The dam with 2H:1V upstream slope was selected for this analysis under three cases: tailings replaced by an equivalent pressure, tailings with $V_{s1} = 10$ m/s, and tailings with $V_{s1} = 100$ m/s. The value of the mass, m, used in the analysis corresponds to the mass of the dam per unit length, based on its cross-sectional area and density, while the spring constant, *k*, was adjusted to fit the vibration period of the horizontal acceleration during free vibration. The value of the damping, *c*, varied in each case to fit the vibration amplitude decay.

The comparison between the 2D numerical model response and the fitted SDOF equations is presented in Figure 21, showing an excellent match considering constant values of *m* and *k*, confirming the validity of evaluating the tailings damping ratio contribution as $\xi_{tailings} = \xi_{total} - \xi_{foundation}$. The analysis also indicates that the damping increases with the tailings stiffness, which is consistent with the results previously presented.

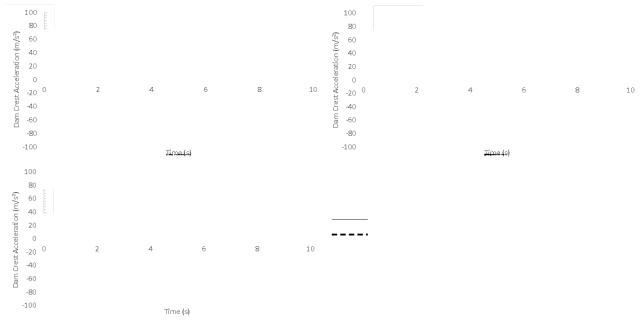

Figure 21. Dam crest acceleration comparison between 2D numerical model and SDOF model for 2H:1V dam upstream slope: a) Tailings modeled as an equivalent pressure, b) Tailings with $V_{s1} = 10$ m/s, c) Tailings with $V_{s1} = 100$ m/s.

6 RADIATION DAMPING EFFECT IN THE DAM DYNAMIC RESPONSE

The radiation damping has been evaluated for different dam configurations and material properties, including the tailings in the impoundment, the dam upstream slope, and the foundation material. With the objective to assess the effect of the radiation damping on the dam dynamic response, the ratio between the maximum horizontal crest acceleration over the maximum input acceleration, $A_{max\_Crest}/A_{max\_Input}$, are analyzed for the numerical models previously described, as shown in Figure 22. The large amplification of the accelerations is consistent with the linear elastic modeling of the materials, being the radiation the only source of damping.

Figure 22a presents the effect that the radiation damping through the impoundment has over the dam dynamic response for the different conditions of the tailings, expressed by the V_{s1} value. These results are from the models where the bedrock has a shear wave velocity of $V_s = 2000$ m/s, and a 2H:1V upstream dam slope. As expected, the $A_{max\_Crest}/A_{max\_Input}$ ratio decreases when the tailings stiffness increases, along with the radiation damping through the tailings.

The effect of the foundation stiffness in the dam dynamic response is evaluated and presented in Figure 22b, showing an increase in the $A_{max\_Crest}/A_{max\_Input}$ ratio as the foundation stiffness increases, with the corresponding decrease of the radiation damping through the dam base. The models used for this comparison consider that the dam upstream slope is 2H:1V and the tailings shear wave velocity is $V_{s1} = 10$ m/s.

Figure 22b presents the effect that the radiation damping, resulting from different dam upstream slopes, has over the dam dynamic response. These results consider that the bedrock has a shear wave velocity of $V_s = 2000$ m/s, and the tailings in the

impoundment are represented by a shear wave velocity V_{s1} = 10 m/s.

There is a significant variation of the $A_{max\_Crest}/A_{max\_Input}$ ratio between the extreme cases considered: the 2H:1V upstream slope and the dam with centerline raise in stages, showing the impact that the dam design has over the radiation damping to reduce the dam dynamic response.

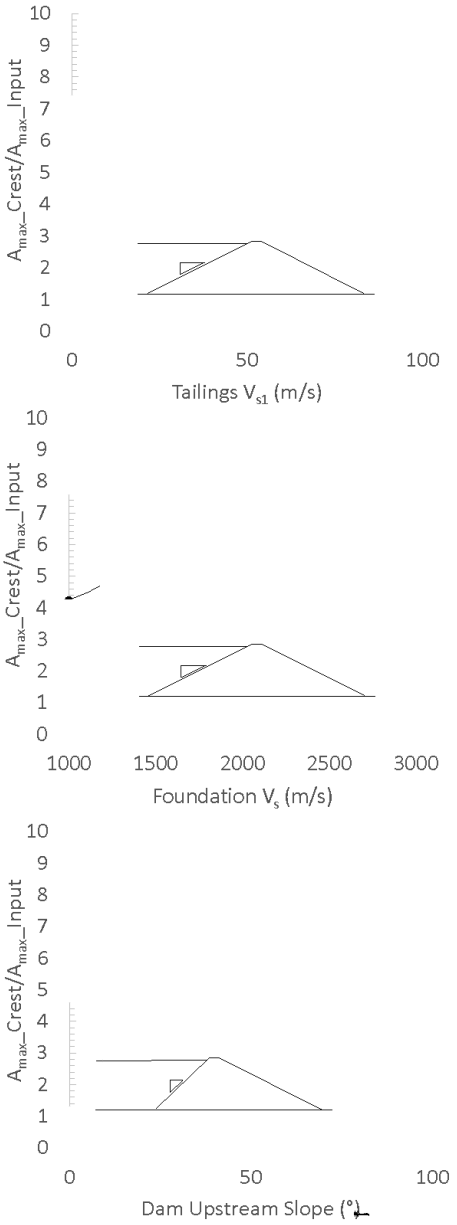

Figure 22. $A_{max\_Crest}/A_{max\_Input}$ ratio: a) Variation with tailings V_{s1}, b) Variation with foundations V_s, c) Variation with dam upstream slope.

From Figure 22, it is clear that the stiffness of the impoundment and foundation materials, and the dam upstream slope, have a non-negligeable effect on the dam dynamic response. The effort associated with the geotechnical characterization of the tailings in the impoundment and the foundation materials, particularly regarding their stiffness and the variation of their stiffness during a dynamic loading, should not be understated, and simplified assumptions should be avoided.

8 CONCLUSIONS

Several numerical models were carried out representing a simple configuration of a TSF, under different dam upstream slopes and different tailings and foundation material properties. The purpose of the models was to evaluate and quantify the radiation damping that the foundation and the tailings in the impoundment provide to the dam in a Tailings Storage Facility. The main conclusions are:

a) The radiation damping may be an important contribution to the dam seismic performance, reducing its dynamic response and subsequent accelerations, potentially reducing the dam permanent deformations. For the cases studied, the radiation damping ratio could be as high as 20%.

b) The radiation damping increases for softer foundation materials and increases for stiffer tailings materials. The results show the importance of correctly modeling the stress-strain behavior of the foundation materials, and the tailings materials, when conducting a dynamic deformation analysis of a tailings dam.

c) The tailings radiation damping contribution increases with steeper upstream slopes of the dam. This is a factor that may be relevant for the design of tailings dam in zones subjected to large earthquakes.

d) The impact of the radiation damping was evaluated in terms of the dam´s dynamic amplification of the horizontal accelerations and case-history was analyzed. The results confirm the significant effect of the radiation damping contribution to the overall dam dynamic response.

e) The effort associated with the geotechnical characterization of the tailings in the impoundment and the foundation materials, particularly regarding their stiffness and the variation of their stiffness during a dynamic loading, should not be understated, and simplified assumptions should be avoided.

9 REFERENCES

ANCOLD 2019. Guidelines for Design of Dams and Appurtenant Structures for Earthquake. *Australian National Committee on Large Dams*.

Borja, R., & Reyes, A. 2016. Analysis of a Tailings Storage Facility Founded on Soft Clay with High Seismic Conditions. *Proceedings Tailings and Mine Waste 2016* | Keystone, Colorado, USA | October 2-5, 2016.

CDA 2013. Dam Safety Guidelines. *Canadian Dam Association*.

Chakraborty, D., & Choudhury, D. 2011. Seismic behavior of tailings dam using flac3d. In Geo-Frontiers 2011: *Advances in Geotechnical Engineering* (pp. 3138-3147).

Ferdosi, B., James, M., & Aubertin, M. 2015. Effect of waste rock inclusions on the seismic stability of an upstream raised tailings impoundment: a numerical investigation. *Canadian Geotechnical Journal*, 52(12), 1930-1944.

Itasca 2019. FLAC — Fast Lagrangian Analysis of Continua, Ver. 8.1. Itasca Consulting Group, Inc. Minneapolis.

Kramer, S. L. 1996. Geotechnical earthquake engineering. Prentice Hall, N.J.

Naeini, M., & Akhtarpour, A. 2018. Numerical analysis of seismic stability of a high centerline tailings dam. *Soil Dynamics and Earthquake Engineering*, 107, 179-194.

Paull, N. A., Boulanger, R. W., & DeJong, J. T. 2020. Accounting for spatial variability in nonlinear dynamic analyses of embankment dams on liquefiable deposits. *Journal of Geotechnical and Geoenvironmental Engineering*, 146(11).

Psarropoulos, P. N., & Tsompanakis, Y. 2008. Stability of tailings dams under static and seismic loading. *Canadian Geotechnical Journal*, 45(5), 663-675.

Richart Jr, F. E., & Whitman, R. V. 1967. Comparison of footing vibration tests with theory. *Journal of the Soil Mechanics and Foundations Division*, 93(6), 143-168.

SERNAGEOMIN 2007. Reglamento para la Aprobacion de Proyectos de Diseño, Construcción, Operación y Cierre de los Depósitos de Relaves. Gobierno de Chile - *Ministerio de Minería*.

Shuttle, D., Marinelli, F., Brasile, S., & Jefferies, M. 2021. Validation of computational liquefaction for tailings: Tar Island slump. *Geotechnical Research*, 9(1), 32-55.

Vargas, C. O. 2019. Analysis and Seismic Design of Tailings Dams and Liquefaction Assessment. *In American Conference on Soil Mechanics and Geotechnical Engineering* (Vol. 7, p. 392).

Villavicencio, A. G., Breul, P., Bacconnet, C., Boissier, D., & Espinace, A. R. 2011. Estimation of the variability of tailings dams properties in order to perform probabilistic assessment. *Geotechnical and Geological engineering*, 29(6), 1073-1084.

Youd, T. L., & Idriss, I. M. 2001. Liquefaction resistance of soils: summary report from the 1996 NCEER and 1998 NCEER/NSF workshops on evaluation of liquefaction resistance of soils. *Journal of geotechnical and geoenvironmental engineering*, 127(4), 297-313.